PHYSICAL REVIEW B VOLUME 47, NUMBER 18 1 MAY 1993-II

Local structure of Co- and Fe-substituted $YBa_2Cu_3O_{7-\delta}$ studied by x-ray-absorption spectroscopy

G. G. Li and F. Bridges
Physics Department, University of California, Santa Cruz, California 95064

J. B. Boyce
Xerox Palo Alto Research Center, Palo Alto, California 94304

W. C. H. Joiner
Physics Department, University of Cincinnati, Cincinnati, Ohio 45221-0011

(Received 8 October 1992)

We have used the x-ray-absorption fine-structure technique to investigate the local structure about Cu and Co atoms in $YBa_2(Cu_{1-x}Co_x)_3O_{7-\delta}$, processed with different thermal treatments, for $x = 0.05$, 0.08, 0.10, 0.11, and 0.30. Some investigators have suggested that a high-temperature anneal in the absence of oxygen, followed by a low-temperature anneal in oxygen will move Co from the chain site (Cu(1)) to the plane site (Cu(2)). We find no evidence for a movement of Co to the Cu(2) site for this thermal treatment for any of the concentrations studied. Similar results were also obtained from one Fe substituted sample. Our analysis indicates that Co/Fe occupies a strongly distorted Cu(1) site in which CoO_z (FeO_z) clusters are displaced relative to the rest of the lattice.

I. INTRODUCTION

Since the discovery of the high-T_c superconductor $YBa_2Cu_3O_{7-\delta}$ (Y-Ba-Cu-O), 3*d*-metal substitutions for Cu have been extensively studied in an effort to understand the relevance of various structural features, such as the two different Cu-O layers, to superconductivity. The valence and magnetic properties of substituted cations have also been investigated. However, in all such investigations, the analysis of the local structure about dopant atoms on the Cu sites is complicated by the fact that two distinct Cu sites exist in Y-Ba-Cu-O (see Fig. 1 for the definition of the various sites). For Co-doped Y-Ba-Cu-O, neutron-diffraction,[1–5] x-ray-absorption fine-structure (XAFS),[6–8] differential anomalous x-ray-scattering,[9] and Raman-spectroscopy[10–12] studies have all shown that Co preferentially occupies the Cu(1) site in the CuO chains. Mössbauer studies[13] also indicate a preference for Co substitution on the Cu(1) site in $YBa_2Cu_3O_7$, although the interpretation[14] of one experiment for $YBa_2Cu_3O_6$ has the Co atoms mainly on the Cu(2) site in the CuO_2 planes.

A few years ago, several investigators showed that Fe- and Co-substituted samples could be prepared so that they remain orthorhombic to high Co/Fe concentrations, above 10 at. %.[15,16] The samples first undergo a high-temperature anneal in an oxygen-deficient environment (> 700 °C) which removes oxygen. This is followed by a low-temperature ($\approx 400\,°C$) anneal in an O_2 environment which reintroduces oxygen. In addition it has been suggested that during the high-temperature anneal in the absence of O, the Co and Fe atoms move to the Cu(2) site in $YBa_2Cu_3O_7$ (Refs. 17 and 18) to achieve a higher O coordination, and are trapped there when the samples are reoxygenated. However, not all experiments come to this conclusion.[19,20] Furthermore, recent Mössbauer experiments[21] on $Y_{1-z}Ca_zBa_2(Cu_{1-x}Co_x)_3O_7$ suggest that this type of annealing process has the opposite effect for Co-substituted samples codoped with Ca—i.e., Co(2) tends to be moved to Co(1).

Another important question concerns the local structure about the Co(1) atom. Is it essentially the same as the usual Cu(1) environment or are there significant distortions? Four XAFS studies[6–8,22] have different answers. In a previous study,[6] we have shown that Co and Fe substitute primarily at the Cu(1) site, in agreement with other investigations. More importantly, however, we find that many of the substituted sites are significantly distorted, with some of the Co (or Fe) atoms displaced (probably along the ⟨110⟩ direction) from the position a Cu(1) atom would normally occupy. Since the Co-O nearest-neighbor bonds are not strongly disordered, it is a CoO_z cluster that is displaced relative to the rest of the lattice. Similar distortions of the Co(1) site have recently been reported by Renevier, Hodeau, and Marezio.[8] Yang *et al.*[7] find no evidence for a distortion of the Co(1) and Fe(1) sites but do not analyze in detail the further Co(1) neighbors, which show the largest effects of the distortion. Padilia *et al.*[22] also report no evidence for a distortion but used only a single peak, with a very large width, for the Co-Ba contribution. The large width indicates considerable disorder of the Co relative to the Ba atoms.

Here, we have used the x-ray-absorption fine-structure (XAFS) technique[23,24] to probe the local structure around Cu, Co, and Fe in Y-Ba-Cu-O, to check our earlier results and to investigate possible movement of the Co to the Cu(2) site via the thermal treatment (vacuum

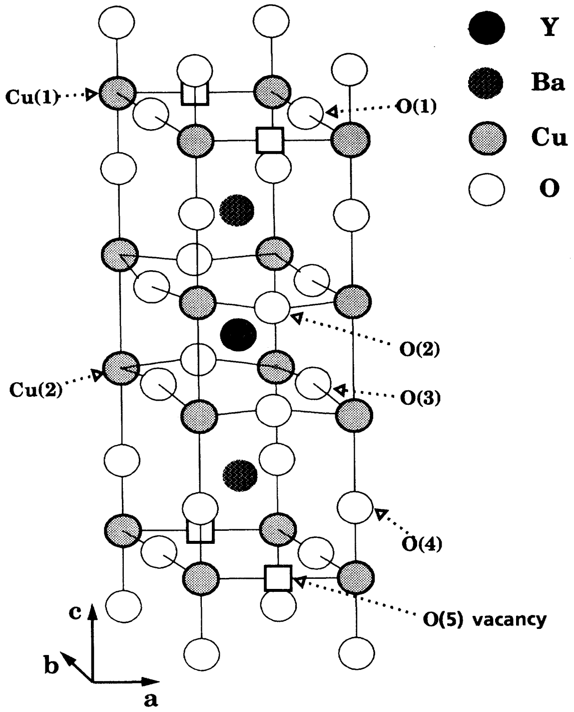

FIG. 1. Crystal structure for Y-Ba-Cu-O showing the definitions for the different Cu and O sites. From Ref. 6, with permission.

anneal plus reoxidization) described above. A large number of samples have been studied, and an improved data analysis procedure has been used. The sample preparation and experimental details of our XAFS measurements are described in Sec. II and our modified XAFS data analysis discussed in detail in Sec. III. The XAFS data and the data analysis for the Cu and Co/Fe *K* edges are presented in Secs. IV and V, respectively, followed by a short discussion of the near-edge structure in Sec. VI. A comparison of our results with other experiments on substituted Y-Ba-Cu-O materials is given in Sec. VII and our conclusions summarized in Sec. VIII.

II. SAMPLES AND EXPERIMENTS

A. Sample preparation

The powder samples, with various Co concentrations, were prepared in a standard way, starting with a sintering of a mixture of metal-oxide powders in air, for 40 h at 950 °C. The material was reground and sintered three more times, with shorter anneals of 10 or 15 h, carried out in flowing oxygen. In each case the cooldown time following an anneal was very long (13–60 h). Vacuum anneals were done using a maximum temperature of 750 °C for 1/2 h, plus 12 h to cool from 750 to 690 °C. In each case the samples were heated up and cooled down slowly. The final step of reoxygenation was carried out in O_2 gas at 390–410 °C (20+ h) followed by a slow cooldown to room temperature. The samples that undergo a high-temperature vacuum anneal to remove oxygen followed by a low-temperature oxygenation will be referred to as "reoxidized" in this paper. Details regarding the Co/Fe concentration, the resulting value of T_c as determined by dc susceptibility, and the lattice constants from x-ray diffraction are given in Table I. One Fe-substituted sample is also included in this study.

B. XAFS samples

The XAFS samples were prepared by brushing a fine powder (≈ 30 μm) onto Scotch tape. Several layers were stacked to obtain a sample with a thickness of approximately two absorption lengths. Each sample was selected to be free of pinholes and measured at 80 K using a liquid-nitrogen Dewar. For all samples, several data sets were collected to check for consistency; for the lower-concentration samples, many data sets were collected and averaged to improve the signal-to-noise ratio. The x-ray-absorption data were collected on the

TABLE I. Sample information: Co (Fe) concentration, thermal treatment, lattice constants, and the value of T_c from dc susceptibility.

Sample	Co/Fe conc.	Treatment	a (Å)	b (Å)	c (Å)	T_c (K)
1	5 at.% Co	untreated	3.861	3.861	11.672	77.2
2	5 at.% Co	reoxidized	3.835	3.888	11.671	83.2
3	8 at.% Co	untreated	3.867	3.867	11.680	58.3
4	8 at.% Co	reoxidized	3.849	3.883	11.667	61.6
5	10 at.% Co	untreated	3.872	3.872	11.678	47.7
6	10 at.% Co	vac. anneal				0
7	10 at.% Co	reoxidized	3.852	3.883	11.662	35.7
8	11 at.% Co	untreated	3.873	3.873	11.677	38.5
9	11 at.% Co	reoxidized	3.870	3.870	11.664	38.8
10	30 at.% Co	untreated	3.890	3.890	11.635	0.0
11	30 at.% Co	vac. anneal				0.0
12	30 at.% Co	reoxidized	3.888	3.888	11.626	0.0
13	7.5 at.% Fe	untreated	3.866	3.866	11.671	70.0
14	7.5 at.% Fe	reoxidized	3.838	3.877	11.669	70.4

wiggler beam line 4-1 at the Stanford Synchrotron Radiation Laboratory using Si(220) monochromator crystals. The double monochromator was detuned on its rocking curve to approximately one-half of maximum transmitted x-ray intensity to reduce the harmonic content of the beam, and a leveling feedback system[25] was used to control the piezoelectric crystal of the monochromator to keep the incident photon flux constant. Twelve Co-substituted samples were investigated, five untreated, five reoxidized, and two samples (for 10 and 30 at. % Co) of the vacuum-annealed material. Two Fe-substituted samples (untreated and reoxidized) for 7.5 at. % Fe are also included.

III. XAFS DATA ANALYSIS TECHNIQUE

A. Standard procedures

The reduction and analysis of the XAFS data usually proceeds as follows.[23] First, a polynomial fit to the pre-edge data is subtracted from the entire data set. This polynomial is constrained such that after the subtraction, the remaining data above the absorption edge have the average energy decrease expected from the MacMaster data. This ensures that the normalization by $\mu_0(E)$, described below, is correct. Next the background above the edge is fit to a series of splines or a polynomial and the XAFS function $\chi(E)$ is obtained by the equation $\chi(E) = [\mu(E) - \mu_0(E)]/\mu_0(E)$, where the absorption cross section $\mu(E)$ includes both the absorption edge and the XAFS oscillations and $\mu_0(E)$ (above the edge) is the free atomic absorptance, simulated here to lowest order by the background fit. Then, $\chi(E)$ is converted to k space, using $k = [2m(E - E_0)]^{1/2}/\hbar$, where E_0 is the energy at one-half the absorption edge height. Hence, we extract the modulation function $k\chi(k)$ given by[23]

$$k\chi(k) = \sum_j \frac{N_j F_j(k)}{R_j^2} \sin[2kR_j + \phi_j(k)] \times \exp(-2k^2\sigma_j^2 - 2R_j/\lambda), \tag{1}$$

where the sum is taken over shells with N_j atoms at a distance R_j from the absorbing atom, $F_j(k)$ is the backscattering amplitude, dependent on the kind of atom in shell j, $\phi_j(k)$ is a phase shift depending upon both the backscattering and absorbing atoms, λ is the effective electron mean free path, and σ_j^2 is the mean-square fluctuation of R_j. Examples of the k-space data are given in Fig. 2 for the 10 at. % Co sample, for both the Cu and Co K edges.

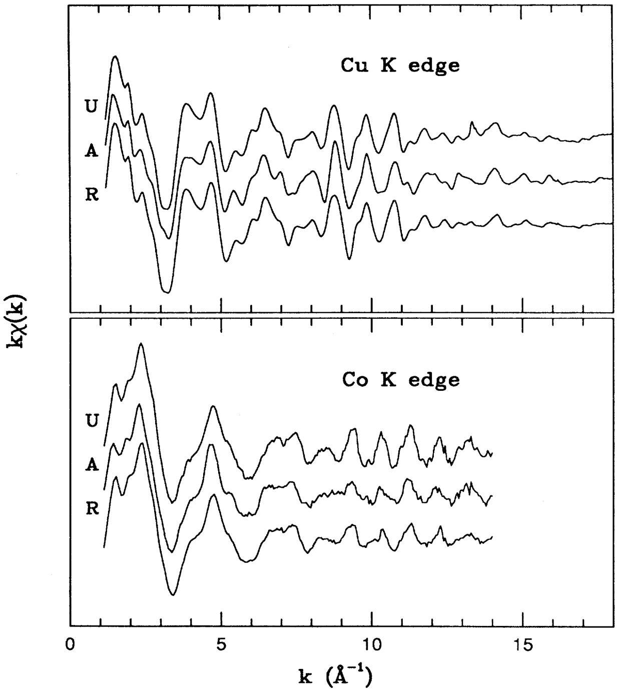

FIG. 2. Extracted XAFS function $k\chi(k)$ for the 10 at. % Co samples, for data collected at the Cu and Co K edges. U, A, and R stand for untreated, vacuum annealed, and reoxidized.

Finally, $k\chi(k)$ is Fourier transformed into real (r) space, using as long a k interval as possible. To obtain numerical values for R_j, N_j, and σ_j, we perform iterated least-square fits of the real and imaginary parts of the Fourier transform of $k\chi(k)$ to a sum of standards for a fixed range of r. Identical k-space transforms are used for the sample and the standards. In these fits, the overlaps of the radial distributions of neighbors in r space are included. We have generally used experimentally determined standards, extracted from compounds with a well-defined and simple local environment. In the extraction process, the contributions to the r-space peak(s) from further neighbors are subtracted to obtain a standard that corresponds to a peak for a single pair of atoms.[6,26,27] In cases where such a standard is not readily available, a standard for a pair of atoms, with atomic numbers near those for the atoms of interest, can be modified using the theoretical XAFS program, FEFF,[28] to represent the desired pair. In this paper, the standard Cu-Ba (Co-Ba, Fe-Ba), Cu-Y (Co-Y, Fe-Y), Cu-O (Co-O, Fe-O), and Cu-Cu (Co-Cu, Fe-Cu) are from Cu-I, Cu-Br, Cu-O, and Cu-Cu, respectively.

The standards used in the present study are very similar to those used earlier,[6,26] but the data for both the standards and the Y-Ba-Cu-O samples have been reduced in a new way.[29] The background function $\mu_0(E)$ above the edge has been optimized to obtain a monotonic, smooth amplitude function for the Fourier transform of $k\chi(k)$ in the low region of r space, $r < 1.0$ Å. The data in the low-k region now agree very well with the theoretical results.[28] In generating the new experimental standards, more care has been taken in removing further neighbor peaks in the standard compound data to obtain an isolated single-pair standard.

B. Constrained fits

Sometimes, even with high quality experimental data and standards, it is still difficult to obtain excellent fit results, especially when the structure is very complicated. For example, in our earlier work[26] the overall XAFS results agreed very well with the diffraction results.[30,31] However, the Cu(2)-Cu(2) distance (3.35 Å) for the oxygen-depleted Y-Ba-Cu-O was 0.06 Å longer than the diffraction results,[31] while the Cu(2)-Y, Cu(2)-Ba, and Cu(1)-Ba distances agreed well. The problem arises because the Cu(2)-Cu(2) peak is very small and lies underneath the Cu-Ba and Cu-Y peaks. Treating each peak independently leads to too many parameters. One way to reduce the number of independent parameters is to introduce constraints consistent with the known structure. These include using the lattice constants from diffraction measurements and the known general location of the atoms in the unit cell. Such constraints assume that the local structure is the same about all Cu(1) sites and similarly for all Cu(2) sites. When defects are present, some of these constraints must be relaxed. We have used constraints to a limited extent in our earlier work[6,26] but have now done it more extensively.

We take Cu K-edge XAFS data for $YBa_2Cu_3O_7$ as an example to show how the constraints are applied. The diffraction results[32] show that the cluster Cu(1)-O(4)-Cu(2) is colinear. Therefore, we can force the sum of the bond distances for Cu(1)-O(4) (1.85 Å) and Cu(2)-O(4) (2.30 Å) equal to that of the Cu(1)-Cu(2) distance (4.15 Å), which we treat as a virtual variable [because we did not include this Cu(1)-Cu(2) peak in the fit process]. The sum of the projection of the Cu(1)-Ba (3.47 Å) and Cu(2)-Ba (3.38 Å) distances along the c axis are also set equal to this Cu(1)-Cu(2) distance. Similarly, the projection of the Cu(2)-Y (3.20 Å) distance along the c axis must be equal to half of the Cu(2)-Cu(2) (3.37 Å) bond distance. Finally, the intermediate Cu(2)-O(2)/O(3) (1.94 Å), the long Cu(2)-O(2)/O(3) (3.66 Å), and the Cu(2)-Cu(2) (3.37 Å) distances can be tied together. We fit the experimental data in r space up to 4.0 Å. There are nine peaks in this region, but only five distances are independent variables.

Constraints in the coordination numbers (N) and edge shifts (ΔE_0) are also used. The ratios of the N's for the O peaks have been set to that of the coordination numbers obtained in diffraction. Similar constraints on N for the metal peaks (Cu, Y, Ba) are imposed with one exception—the peak corresponding to the in-plane Cu-Cu (3.85 Å) distance has a large amplitude (and also appears to be too long) because of the forward-scattering effect from the intervening O atom. The edge shifts for the O peaks have been set equal as have the shifts for the two Cu-Ba peaks. The peak widths (σ) for the shorter O peaks (1.84 Å and 1.94 Å) and for the two Ba peaks have also been set equal, respectively. This reduces the total number of variables from 36 to 20 for the case of nine r-space peaks. With these constraints, the fit results are not only in excellent agreement with the XAFS data for pure Y-Ba-Cu-O, as shown in the top part of Fig. 3, but also agree very well with the diffraction results[1,4] as indicated in Tables II and III. In a large number of cases the constrained fit is a better fit to the XAFS data than that obtained with a larger number of free parameters. The constraints force the fit towards a particular minimum in parameter space, and the fit is not as easily trapped in some other local minima. In some fits we have held a few parameters constant to reduce the number of parameters further. For example, some ΔE_0's are fixed at a value estimated from an average of ΔE_0 from many data files, and some N's are set at the expected coordination number. Fixing a few parameters in this way to reduce the number of parameters to 17–18 does not significantly change the main results, although it does change the width parameter σ slightly.

IV. Cu ENVIRONMENT

A. Data presentation and qualitative features

In Fig. 4, we show the Cu K-edge, r-space data for untreated and reoxidized Co-substituted $YBa_2(Cu_{1-x}Co_x)_3O_{7-\delta}$ samples with x = 0.05, 0.08,

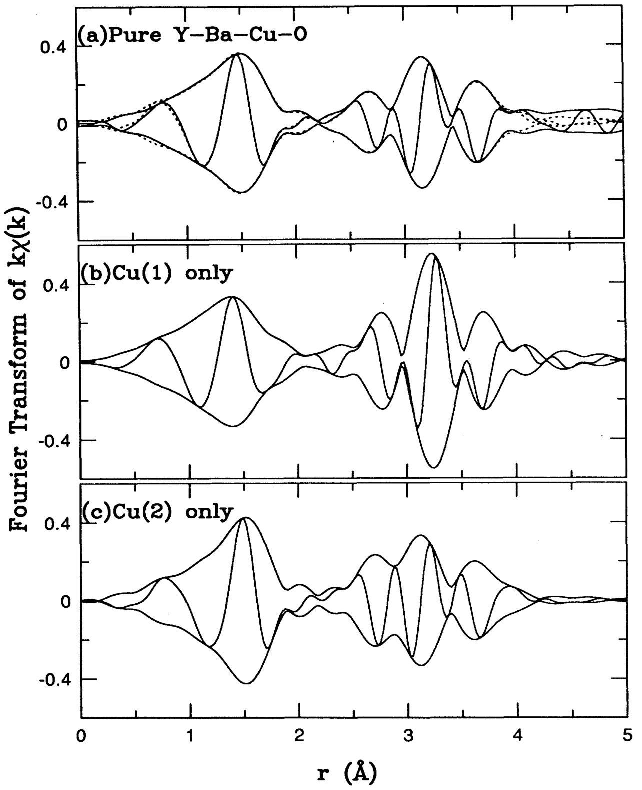

FIG. 3. Fourier transform of $k\chi(k)$ for pure Y-Ba-Cu-O is shown in the top box by the solid line; the dotted line is a fit to the data. The oscillatory function is the real part of the transform and the envelope is given by $(R^2 + I^2)^{1/2}$. The transform window is 3.3–12.5 $Å^{-1}$, Gaussian broadened by 0.3 $Å^{-1}$. In (b) and (c) we show the Cu(1) and Cu(2) contributions normalized for isolated Cu(1) or Cu(2) sites. Note the large amplitude if only a Cu(1) site is occupied. For the Cu(2) site the shape of the second neighbor shell (2.5–4 Å) is strongly dependent on the positions of the Ba and Y atoms, and a small shift of the positions of these atoms can make the Cu(2) site look more like the pure Y-Ba-Cu-O case shown in (a).

0.10, 0.11, and 0.30. The Fourier-transform range is from 3.3 Å^{-1} to 12.5 Å^{-1}, Gaussian broadened by 0.3 Å^{-1}. The data for the untreated and reoxidized samples are almost identical except for the Cu-Ba peaks for the Co-doped samples with $x < 0.12$; the width of the Cu-Ba peaks for the reoxidized sample are consistently narrower than that of the untreated samples. This means that in the low-Co-concentration, reoxidized samples, the Ba atoms are more ordered as viewed from the Cu sites. The first oxygen peak and the peak from Cu neighbors near 3.8 Å are unchanged by the thermal treatment and show the high reproducibility of the data.

Several aspects of the data clearly support the idea that Co atoms are mainly on the Cu(1) sites, in agreement with our earlier results and other studies. The amplitude of the Cu-O peak (near 1.5 Å in the data shown in Fig. 4) increases with the increase in Co content, qualitatively as expected for Co substitution on the Cu(1) site; see Figs. 3(b) and 3(c) for the expected amplitudes of the isolated Cu(1) and Cu(2) sites. The data for the vacuum annealed samples are also consistent with this site assignment (see Fig. 5); the amplitude of the Cu-O peak for the vacuum-annealed, 10 at. % Co sample decreases about 15%, just the decrease expected if all the Co is on the Cu(1) site and the O about the remaining Cu(1) atoms are removed. The amplitude of the Cu-O peak for the untreated 30 at. % Co sample increases as expected (compared to undoped Y-Ba-Cu-O) since most

TABLE II. Cu local structure, from diffraction and from XAFS, with 90% of the Co (or Fe) at the Cu(1) site. "diff" indicates a result from diffraction (Refs. 1, 4, and 32) while *U* and *R* indicate XAFS results for untreated and reoxidized samples. "nbrs" indicates the weighted number of neighbors from XAFS experiments. The number of neighbors listed for diffraction (in parentheses) is the weighted number of neighbors calculated from diffraction results assuming 90% of the Co (Fe) is on the Cu(1) site. The estimated errors are the following: number of neighbors ± 10%; distances, ± 0.02 Å.

	0 at. % Co		5 at. % Co		8 at. % Co		11 at. % Co		7.5 at. % Fe	
Pairs	*r* (Å)	nbrs	*r* (Å)	nbrs	*r* (Å)	nbrs	*r* (Å)	nbrs	*r* (Å)	nbrs
Cu(1)-O(4)										
diff	1.85	(0.67)	1.84[a]	(0.61)		(0.57)		(0.53)	1.84[b]	(0.57)
U	1.85	0.66	1.82	0.54	1.83	0.57	1.83	0.56	1.84	0.53
R			1.84	0.57	1.83	0.56	1.81	0.58	1.84	0.53
Cu(2)-O(2)										
Cu(2)-O(3)										
Cu(1)-O(1)										
diff	1.94	(3.3)	1.94[a]	(3.4)		(3.4)		(3.5)	1.94[b]	(3.4)
U	1.94	3.3	1.93	3.0	1.94	3.5	1.94	3.5	1.93	3.2
R			1.94	3.2	1.94	3.4	1.93	3.6	1.93	3.2
Cu(2)-O(4)										
diff	2.30	(0.67)	2.31[a]	(0.7)		(0.72)		(0.74)	2.32[b]	(0.72)
U	2.30	0.66	2.33	0.62	2.33	0.72	2.34	0.74	2.32	0.67
R			2.31	0.65	2.34	0.72	2.35	0.76	2.32	0.67
Cu(2)-Y										
diff	3.20	(2.7)	3.20[a]	(2.8)		(2.9)		(3.0)	3.20[b]	(2.9)
U	3.20	2.7	3.20	2.8	3.19	2.9	3.19	3.1	3.19	3.0
R			3.2	2.9	3.19	3.0	3.19	3.0	3.19	3.0
Cu(2)-Ba										
diff	3.38	(2.7)	3.39[a]	(2.8)		(2.9)		(3.0)	3.38[b]	(2.9)
U	3.39	2.7	3.39	2.8	3.39	2.9	3.39	3.1	3.40	3.0
R			3.39	2.9	3.39	3.0	3.39	3.0	3.39	3.0
Cu(1)-Ba										
diff	3.47	(2.7)	3.47[a]	(2.4)		(2.3)		(2.1)	3.49[b]	(2.3)
U	3.47	2.7	3.48	2.4	3.49	2.3	3.49	2.3	3.48	2.3
R			3.48	2.5	3.48	2.3	3.49	2.2	3.48	2.3
Cu(2)-Cu(2)										
diff	3.37	(0.67)	3.34[a]	(0.70)		(0.72)		(0.76)	3.35[b]	(0.72)
U	3.37	0.67	3.33	0.70	3.30	0.73	3.30	0.76	3.30	0.74
R			3.33	0.72	3.30	0.74	3.30	0.75	3.30	0.75
Cu(2)-O(2)										
Cu(2)-O(3)										
diff	3.66	(2.7)	3.64[a]	(2.8)		(2.9)		(3.0)	3.65[b]	(2.9)
U	3.65	2.6	3.64	2.5	3.63	2.9	3.63	3.0	3.63	2.7
R			3.64	2.6	3.63	2.9	3.63	2.9	3.63	2.7

[a] Calculated from the weighted average of neutron diffraction data (Ref. 1) for 3.3 and 6.7 at. % Co in Y-Ba-Cu-O.

[b] From neutron-diffraction data for Y-Ba-Cu-O with 10 at. % Fe (Ref. 4).

TABLE III. Cu local structure, from diffraction and from XAFS, with 90% of the Co at the Cu(1) site. "diff" and "diff*A*" indicate results from diffraction for normal and vacuum-annealed samples (Refs. 1 and 32), while *U*, *A*, and *R* indicate XAFS results for untreated, vacuum-annealed, and reoxidized samples. "nbrs" indicates the weighted number of neighbors from XAFS experiments. The number of neighbors listed for diffraction (in parentheses) is the weighted number of neighbors calculated from diffraction results assuming 90% of the Co is on the Cu(1) site. The estimated errors are the following: number of neighbors ± 10%; distances, ± 0.02 Å.

	0 at. % Co		10 at. % Co		30 at. % Co	
Pairs	*r* (Å)	nbrs	*r* (Å)	nbrs	*r* (Å)	nbrs
Cu(1)-O(4)						
diff	1.85	(0.67)	1.82	(0.54)		
diff*A*	1.80	(0.67)				
U			1.81	0.55		
A			1.78	0.57		
R			1.84	0.54		
Cu(2)-O(2)						
Cu(2)-O(3)						
diff	1.94	(3.3)	1.94	(3.5)	1.95[a]	(3.8)
diff*A*	1.94	(2.7)		(2.9)		(3.6)
U	1.94	3.3	1.94	3.4	1.94	4.1
A			1.93	3.1	1.94	3.7
R			1.94	3.4	1.94	4.2
Cu(2)-O(4)						
diff	2.30	(0.67)	2.35	(0.73)	2.38[a]	(0.91)
diff*A*	2.47	(0.67)				
U	2.30	0.66	2.35	0.72	2.44	0.98
A			2.39	0.77	2.46	0.92
R			2.33	0.70	2.42	1.0
Cu(2)-Y						
diff	3.20	(2.7)	3.20	(2.9)	3.20[a]	(3.6)
diff*A*	3.18	(2.7)				
U	3.20	2.7	3.19	3.0	3.19	3.7
A			3.19	3.0	3.19	3.5
R			3.19	3.0	3.19	3.6
Cu(2)-Ba						
diff	3.38	(2.7)	3.39	(2.9)	3.40[a]	(3.6)
diff*A*	3.36	(2.7)				
U	3.39	2.7	3.39	3.0	3.43	3.6
A			3.38	3.0	3.41	3.5
R			3.39	3.0	3.43	3.6
Cu(1)-Ba						
diff	3.47	(2.7)	3.49	(2.2)	3.51[a]	(0.72)
diff*A*	3.57	(2.7)				
U	3.47	2.7	3.49	2.2	3.47	0.72
A			3.51	2.2	3.49	0.69
R			3.49	2.3	3.47	0.72
Cu(2)-Cu(2)						
diff	3.37	(0.67)	3.30	(0.73)	3.25[a]	(0.91)
diff*A*	3.28	(0.67)				
U	3.37	0.67	3.30	0.75	3.25	0.94
A			3.30	0.74	3.25	0.87
R			3.30	0.76	3.25	0.90
Cu(2)-O(2)						
Cu(2)-O(3)						
diff	3.66	(2.7)	3.63	(2.9)	3.62[a]	(3.6)
diff*A*	3.62	(2.7)				
U	3.65	2.6	3.63	2.9	3.62	4.0
A			3.63	3.1	3.62	3.8
R			3.63	2.8	3.62	4.1

[a] From neutron-diffraction data for 21.7 at. % Co in Y-Ba-Cu-O (Ref. 1).

of the remaining Cu is on the Cu(2) site. The decrease in the Cu-O peak amplitude of this sample after vacuum annealing (see Fig. 5) is somewhat larger than expected if all the Co is on a Cu(1) site, suggesting that in the high-concentration sample there may be a small amount of Co(2).

The second neighbor shell also changes with increasing Co concentration, but the changes are small; the most obvious change is a decrease in the dip at 3.4 Å with increasing Co concentration. The shape depends on both the relative amplitudes of the Cu(1)-Ba, Cu(2)-Ba, and Cu(2)-Y peaks and small shifts in the positions of these peaks. A detailed fit is needed to obtain these parameters.

For the 30 at. % Co-doped sample, we would expect a significant change in the Cu K-edge XAFS r-space data if a large fraction of Co moved from the Cu(1) to the Cu(2) site with the thermal heat treatment (vacuum anneal plus reoxidization) discussed above. Conversely, if most of the Co atoms do not move, there will be very little change in the Cu K-edge data. We emphasize the change in the spectrum here, as in a fit to the data, there is always some uncertainty in the peak amplitudes because the amplitude and the peak width parameters are coupled. Experimentally for the 30 at. % Co sample, there is very little difference in the data between the untreated and reoxidized samples (see lower part of Fig. 4). The solid and dashed lines overlap so closely that the dashed line cannot be seen. In Fig. 6 we show an enlargement of this data to show how well these two spectra overlap. The r-space data for the untreated and reoxidized 30 at. % Co samples are virtually identical, indicating that there is very little movement of Co from one site to another. In contrast, there is a clear difference in the XAFS data between these samples and the vacuum annealed samples (see Fig. 5). Thus on a qualitative level these data indicate a Co(1) substitution site and little change of site with thermal treatment. To make numerical comparisons, we must carry out detailed fits as described in the next section.

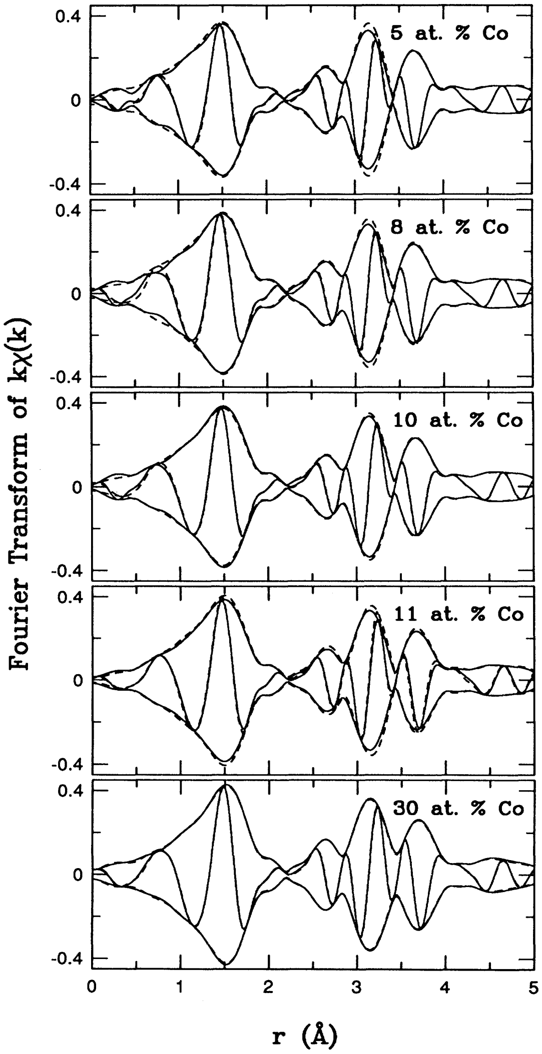

FIG. 4. Fourier transform of $k\chi(k)$ at the Cu K edge for the different Co substituted samples. The solid line is for untreated, and the dashed line for the reoxidized samples. Transform range is 3.3–12.5 $Å^{-1}$, Gaussian broadened by 0.3 $Å^{-1}$.

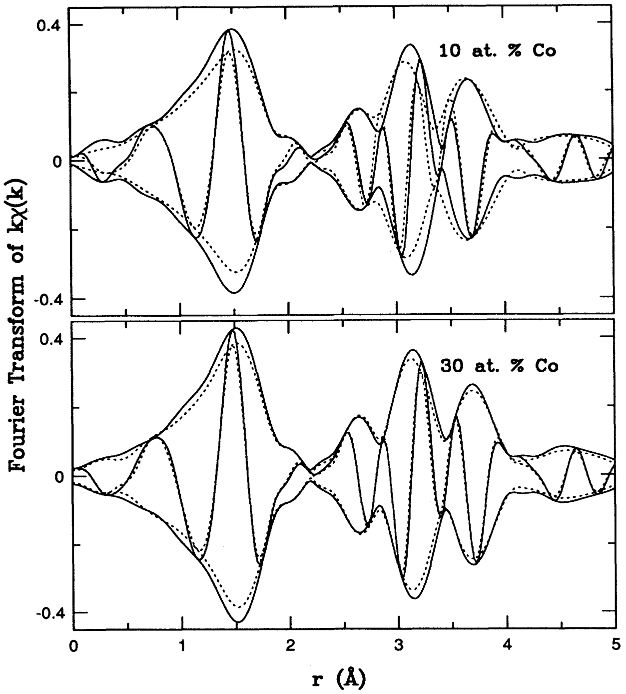

FIG. 5. Comparison of the Fourier transforms of $k\chi(k)$ at the Cu K edge for the untreated (solid line) and vacuum-annealed (dotted line) samples with 10 and 30 at. % Co. Transform range is 3.3–12.5 $Å^{-1}$, Gaussian broadened by 0.3 $Å^{-1}$.

B. Detailed data analysis

There are two different Cu sites in Y-Ba-Cu-O (see Fig. 1 and Tables II and III). For Cu(1), there are two

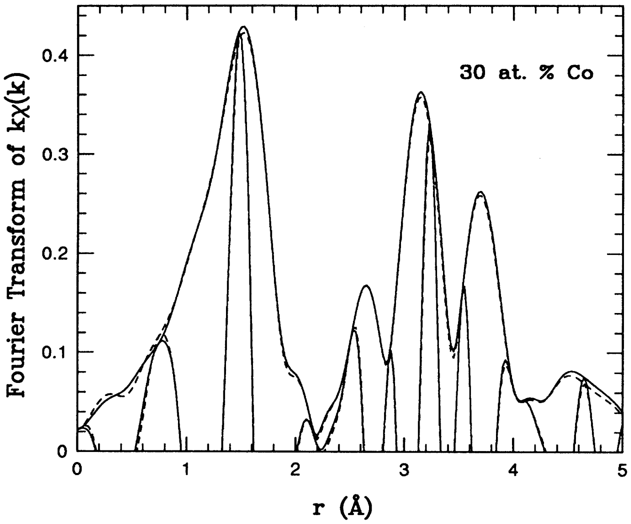

FIG. 6. Enlargement of the Fourier transform of $k\chi(k)$ at the Cu K edge, for the 30 at. % Co sample, illustrating the lack of change between the untreated (solid) and reoxidized (dashed) samples.

O neighbors at 1.85 Å, two O neighbors at 1.94 Å, eight Ba neighbors at 3.47 Å, and four Cu neighbors in the range 3.82–3.88 Å. For Cu(2), there are four O neighbors near 1.95 Å, one O neighbor at 2.30 Å, four O neighbors at 3.66 Å, four Y neighbors at 3.20 Å, one Cu(2) neighbor at 3.37 Å, four Ba neighbors at 3.38 Å, and four Cu(2) neighbors in the range 3.82–3.88 Å. The total amplitude of each of the atom pairs determined by XAFS is the weighted number of neighbors on the two sites.[6] For the substituted sample, the total amplitude is again a weighted average, but now we must include the fractional occupation of each type of site.

For example, consider the 30 at. % Co sample and assume that 90% of the Co atoms are on the Cu(1) site. It is useful to think in terms of layers, with three Cu layers present in pure Y-Ba-Cu-O. Then for the above sample the number of layers of Cu(2), Cu(1), Co(2), and Co(1) are 1.91, 0.19, 0.09, and 0.81. The weighted number of Ba neighbors are Cu(1)-Ba [$8\times0.19/(1.91+0.19)$] $=0.72$; Cu(2)-Ba, 3.6; Co(1)-Ba, 7.2; etc. Note that with most of the Co on a Co(1) site the weighted number of Ba neighbors about Co is much *larger* than for Cu in Y-Ba-Cu-O [the Cu(1) site has eight Ba neighbors compared to four Ba neighbors for the Cu(2) site]. For the vacuum-annealed samples, we assume that all of the O(1) atoms, adjacent to Cu(1) atoms, have been removed. In Tables II and III, the calculated results, assuming 90% of the Co atoms are on the Cu(1) site, are included in brackets. In discussing the data we will often refer to the peak from 1 to 2 Å as the first neighbor shell (composed of three O bonds) and the multipeak from 2 to 4 Å as the second shell. The latter is formed from Cu-Y, Cu-Ba, Cu-Cu, and a long Cu-O distance.

The primary question we are addressing is the distribution of Co on the Cu(1) and Cu(2) sites in bulk material before and after thermal processing. For low concentrations of Co in Y-Ba-Cu-O, the calculated weighted number of Cu neighbors is not very sensitive to the distribution function. For example, the weighted coordination number for Cu(2)-Ba only changes from 3.0 to 2.7 for the 10 at. % Co-doped sample when the distribution of the Co atoms on Cu(1) site changes from 100% to 50%. Thus the Cu K-edge data give little information about the Co distribution function for low Co concentrations. However, it is possible to estimate the distribution for the 30 at. % Co-doped samples. We have tested several distributions of the Co atoms for these samples. The Fourier-transform range is from 3.3 Å^{-1} to 12.5 Å^{-1}, Gaussian broadened by 0.3 Å^{-1}, and the fit range in r space is from 1.1 Å to 3.9 Å. In these fits to the Cu K-edge data, we include many of the constraints described in the previous section plus an assumption on the fraction of Co on the Cu(1) site. Fits are repeated for several different Co distribution assumptions.

The similarity of the second neighbor shell of the 30 at. % Co sample with that of pure Y-Ba-Cu-O (see Figs. 3 and 4) indicates little distortion of the lattice as viewed from the Cu site; in particular, the Ba atom bond lengths do not have a large increase in σ. However, the constraints that linked the Cu(1)-O(4)-Cu(2) distance with the c-axis projections of the Cu(1)-Ba and Cu(2)-Ba bond lengths are no longer valid. The Cu(1)-O(4) contribution is relatively small in pure Y-Ba-Cu-O. If most of the Co replaces Cu(1), the amplitude of the remaining Cu(1)-O(4) r-space peak is very small and we remove this peak from the fit. Our fits clearly show that for the 30 at. % Co sample, a distribution of 70%–100% of the Co on the Cu(1) site gives the best overall fit; the results are essentially the same within these limits [the fits with 80–90 % Co(1) are slightly better]. For more Co on the Cu(2) site, the quality of fit decreases significantly, the peak amplitudes differ from the predicted numbers, and in some cases the widths become unreasonable. We use 90% Co on the Cu(1) sites as a reasonable distribution for this high-Co-concentration sample for comparison purposes.

The distances from the Cu atoms determined by XAFS fits and by diffraction,[1,4] and the corresponding weighted amplitudes from XAFS fits, with the assumption that 90% of the Co atoms are on the Cu(1) site, are shown in Tables II and III. For the low-Co-concentration samples, the numbers of Cu neighbors differ very little between 90% and 100% Co(1). The distances and amplitudes of the Cu(2) neighbors for all the samples and the Cu(1) neighbors for the low-Co-content samples ($x<0.12$) are in excellent agreement with the diffraction results. The only exception is the long, ab-plane Cu-Cu bond (not included in the table) which appears to be too long because multiple scattering from the intervening O atom is not included.[6,26] The amplitude of the Cu(1)-Ba peak for the 30 at. % Co samples is larger than expected for 100% of the Co on the Cu(1) site but is consistent with 90% of the Co on Cu(1). The Cu(1)-Ba distance for these samples differs slightly from the diffraction results, because the diffraction experiment only gives the average results over Cu and Co atoms. The quality of the fits is excellent (see Fig. 7) as shown by the agreement between the

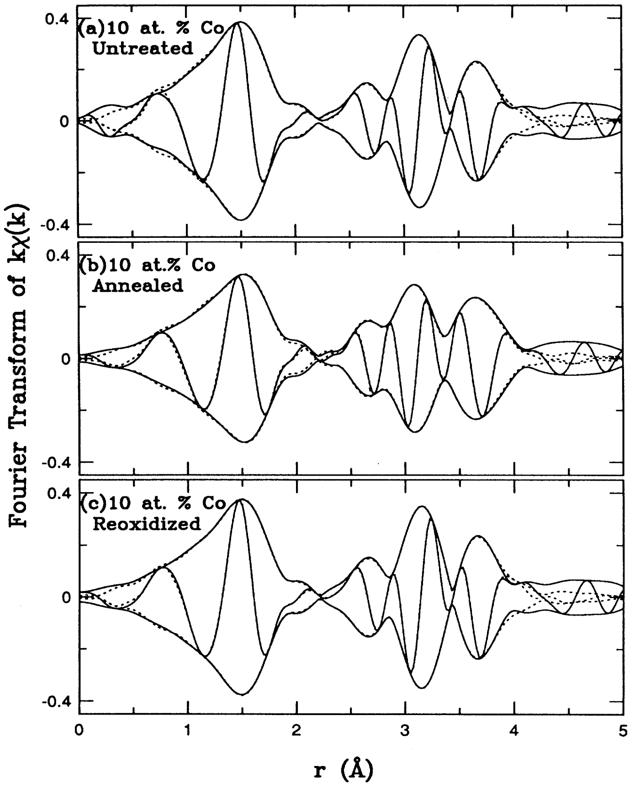

FIG. 7. Examples of fits to the Cu K edge r-space data for the 10 at. % Co sample showing the high quality of the fit. Solid line, data; dotted line, fit over range 1–4 Å.

calculated curve (dotted lines) and the data (solid line) for $x = 0.10$.

From Tables I, II, and III, the following general overall points should be noted.

(1) With increasing Co content, the c axis decreases; the CuO_2 planes move together, but the Cu(2)-Y distance remains nearly the same, consistent with a slight increase in the average of the a and b lattice parameters. The separation between the chains and planes increases a little, and O(4) moves away from Cu(2). All of these points are in good agreement with the neutron-diffraction results.[1]

(2) The Cu local structure for the untreated and reoxidized samples is very similar. After the vacuum annealing, the O in the Cu chains has been removed; O(4) moves away from Cu(2) and Ba towards the CuO_2 plane, which are similar to the oxygen-deficient pure Y-Ba-Cu-O results.[26]

(3) Good fits can be achieved to the Cu XAFS data for all the Co-doped samples with 90% of the Co on the Cu(1) site; for the low Co concentrations it is quite likely that 100% of the Co is on the Cu(1) site. There is no significant evidence in the Cu K-edge data, particularly for the 30 at. % Co sample, that indicates that a large fraction of the Co moves between the Cu(1) and Cu(2) sites during the thermal treatment.

(4) The Cu local environment of the Co-doped Y-Ba-Cu-O is quite similar to that of pure Y-Ba-Cu-O, which indicates that O, Ba, Y and Cu atoms are in almost the same positions as in the pure sample.

For the Cu K-edge data of the 7.5 at. % Fe-doped sample, we used the same constraints as for the 8 at. % Co-doped sample, since the behavior of Fe and Co in Y-Ba-Cu-O is quite similar.[6] The fit parameters are included in Table II, together with the distances from diffraction[4] and the weighted number of neighbors predicted by the assumption that 90% of the Fe atoms are on Cu(1) sites. Again, the fit with all the Fe on the Cu(1) site is just as good. The high quality of the strongly constrained fit to the experimental data can been seen in Fig. 8.

In XAFS data analysis, the coordination number (N) and the distance (R) are usually coupled with the Debye-Waller factor (σ) and the edge shift (ΔE_0), respectively, which increases the uncertainty in determining these parameters. In addition, pinhole and thickness effects, in both the standard and unknown samples, introduces an extra error in N. However, these errors can be minimized by the constrained fits and calibration procedures. In our data analysis, the constraints for N, R, and ΔE_0 among various pairs greatly reduce the strength of the coupling between N and σ, R and ΔE_0. We have also calibrated the amplitudes of our standards by fitting them to the average data of pure Y-Ba-Cu-O. For the dilute (< 10 at. %) Co samples, where comparisons of the XAFS amplitudes with the coordination numbers obtained from diffraction experiments are possible, these procedures result in an error of about 10% for the number of neighbors. The distances extracted from our constrained fits have much less variation, and in most cases the difference between XAFS and diffraction is less then 0.02 Å. For a few cases the errors in the distance to the further neighbor are slightly larger, 0.04 Å.

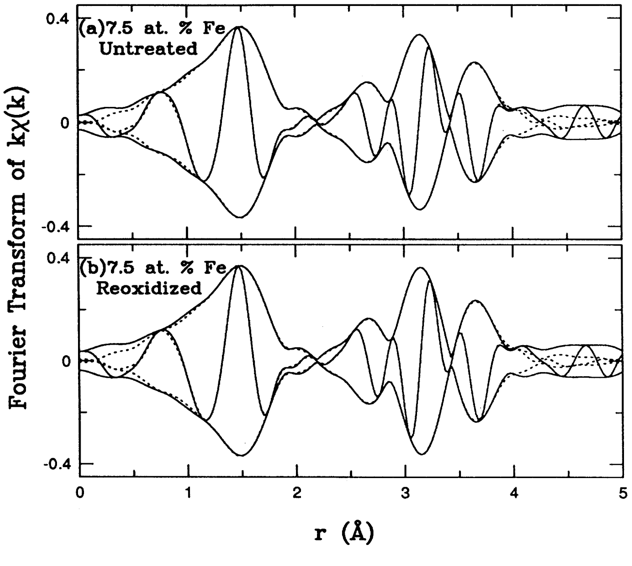

FIG. 8. Cu K-edge r-space data for the Fe-substituted samples (transform window is 3.3–12.5 $Å^{-1}$, Gaussian broadened by 0.3 $Å^{-1}$.) Solid line, data; dotted line, fit.

V. Co AND Fe ENVIRONMENT

A. Data presentation and qualitative features

The Co K-edge XAFS data have been reduced and Fourier transformed in the same way as for the Cu K-edge data. The results are shown in Fig. 9, which has the same vertical scale as in Fig. 4. The shape of the data for the first shell in r space ($r < 2.0$ Å) looks quite similar to that of the Cu K-edge data (See Fig. 4), but the shape of the second shell (2 Å$< r <$ 4 Å) is completely different. The Ba contribution near 3.2 Å is small and shifted slightly, while the Cu component which is at 3.7 Å in pure Y-Ba-Cu-O is nearly absent. The second neighbor shell in the experimental data is also clearly quite different from the simulations of the XAFS data for a Cu/Co atom residing on only an undistorted Cu(1) or Cu(2) site as shown in Fig. 3. The experimental amplitude is too small, which indicates that either the atoms in the second shell or the Co atoms themselves are disordered. Since the Cu K-edge data show only a slight broadening of the second neighbor shell, the small Co amplitude for this shell indicates *disorder* of the Co atoms on a Cu site.

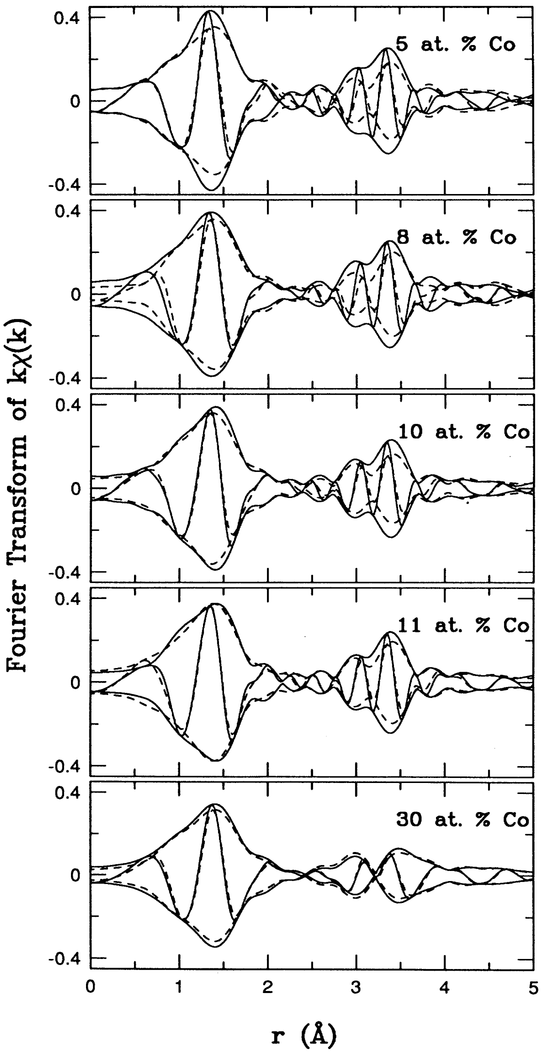

FIG. 9. r-space data at the Co K edge for the Co-substituted samples. The solid line is for the untreated material, and the dashed line is for the reoxidized material. Note the overall small change after reoxidization, for the 30 at. % Co sample.

For the untreated samples, the O-peak amplitude is largest for the 5 at. % Co sample, and monotonically decreases a little as the Co concentration increases. This suggests some increasing disorder with Co concentration. The small second shell peak has a similar shape for the 5–11 at. % Co samples; the amplitude decreases slightly with Co concentration and the dip at 3.15 Å becomes more pronounced with increasing concentration. For the 30 at. % Co sample, the shape of the second neighbor shell peak changes considerably and the dip at 3.15 Å is deep.

In the reoxidized samples, the O-peak amplitude is nearly the same for all the samples with a slightly lower amplitude for the 30 at. % Co sample. The variation in amplitude with Co concentration is considerably less than for the untreated samples. The thermal treatment (vacuum anneal plus reoxidation) also results in a large decrease in the amplitude of the second neighbor peak for each of the 5–11 at. % Co samples, although the *shape* of the real part of the transform remains almost unchanged. The amplitude decrease suggests a broadening of the peaks that are present in the untreated sample. This is in contrast to the Cu K-edge data for which the Ba peak became slightly narrower (larger) in the reoxidized samples. This indicates that the disorder is *on the Co site* and not on the Ba site. The small amplitude in the range 2.5–3.0 Å is also at variance with the presence of a large additional Co-Y peak as would be required if a major fraction of the Co moved to the Cu(2) site. We emphasize that for the 30 at. % Co samples, the amplitudes of both the O peak and the small second neighbor peak are almost identical for the untreated and reoxidized materials, indicating little change in the environment about the Co atoms with thermal processing. This is consistent with the Cu K-edge data shown in Fig. 6.

The data for the vacuum annealed samples (10 and 30 at. % Co) are compared with the corresponding data for the untreated samples in Fig. 10. Here the O peak for 30 at. % Co is unchanged, while the peak amplitude decreases about 9% for the 10 at. % Co sample. This is in sharp contrast to the 50% decrease expected for a Cu(1) site in O-deficient Y-Ba-Cu-O. These results indicate that the number of nearest-neighbor O atoms about the Co atom does not change much (the change for the 30 at. % Co sample is zero) when oxygen is removed from the sample in the high-temperature vacuum anneal. We conclude that the nearest-neighbor O atoms must be tightly bound to the Co atoms.

B. Data analysis

Our analysis of the Cu K-edge data indicates that the fraction of Co atoms on the Cu(1) sites is close to 100% in the low-Co-concentration samples and greater than 70%

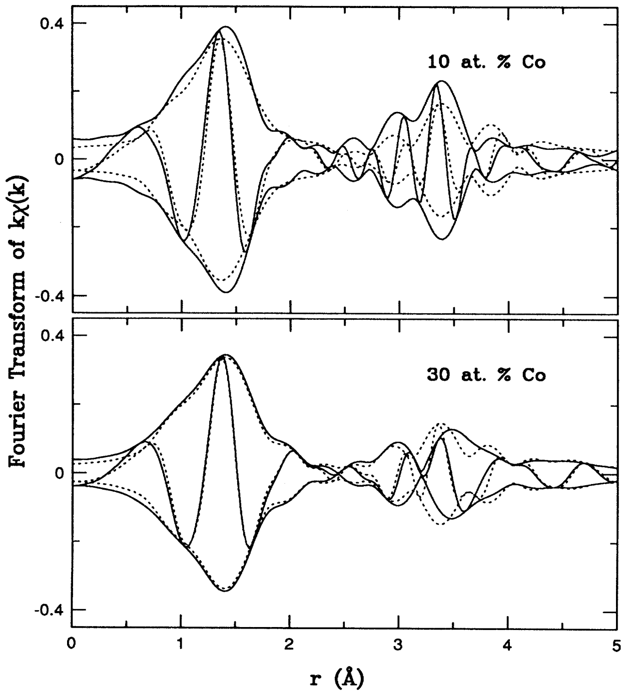

FIG. 10. Co K-edge r-space data for the untreated and vacuum-annealed samples with 10 and 30 at. % Co. Note the large change in shape of the second shell.

(probably closer to 90%) in the 30 at. % Co sample. In addition, from the Cu K-edge data, the Ba, Y, and Cu(2) atoms are close to their normal sites (i.e., the positions in pure Y-Ba-Cu-O) for all of the substituted samples, and the additional broadening is small. Since the amplitude for the second neighbor shell of the Co K-edge data is very small, we conclude that the Co atom must be on a distorted Cu(1) site. Following our previous discussion, we tested the zigzag single and double chain models proposed earlier[6] (see Fig. 11), with more extensive data sets and our more sophisticated analysis technique. For the Co data, the double chain gives a better fit to the data. However, we point out that the chain models are only indicative of the types and magnitudes of the distortions present; the actual distribution of Co is probably much more complicated.

In our fits we first assumed that six or seven peaks were present: two O peaks below 2.5 Å, three Ba peaks, and one or two Cu/Co peaks, consistent with an off-center displacement of roughly 2/3 of the Co atoms along a ⟨110⟩ direction. For a ⟨110⟩ off-center Co atom, two Co(1)-Ba distances are shortened by δr, two distances are lengthened by roughly the same amount, and four distances are essentially unchanged. Including all the Co atoms in the double chain model results in long, medium, and short Co(1)-Ba bonds, having amplitudes in the ratio 1:4:1. We constrained the Co-Ba amplitudes to have this ratio in our fit, and the positions to be r and $r \pm \delta r$. The number of free parameters ranged from 16 to 19. This first fit [which has no Co(2)-Y peak] assumes that all the Co is on the Cu(1) site.

Next we include some Co(2)-Y contribution with a corresponding (constrained) Co(2)-Ba peak. Reasonable fits are obtained with the Co(2)-Y peak amplitude fixed, corresponding to a small amount (0, 10%, or 20%) of the Co on the Cu(2) site. In each case, the second neighbor shell is well described by three Co(1)-Ba peaks separated by $\delta r \approx 0.25$ Å, with the central peak very close to the distance obtained in diffraction measurements [plus, of course, the small fixed Co(2)-Y and Co(2)-Ba peaks required for some Co on Cu(2)]. Variations in the small amount of Co(2)-Y contribution or changes in the peak amplitudes for the longer Co(1)-Cu/Co bonds do not change the results for the Co(1)-Ba peaks very much.

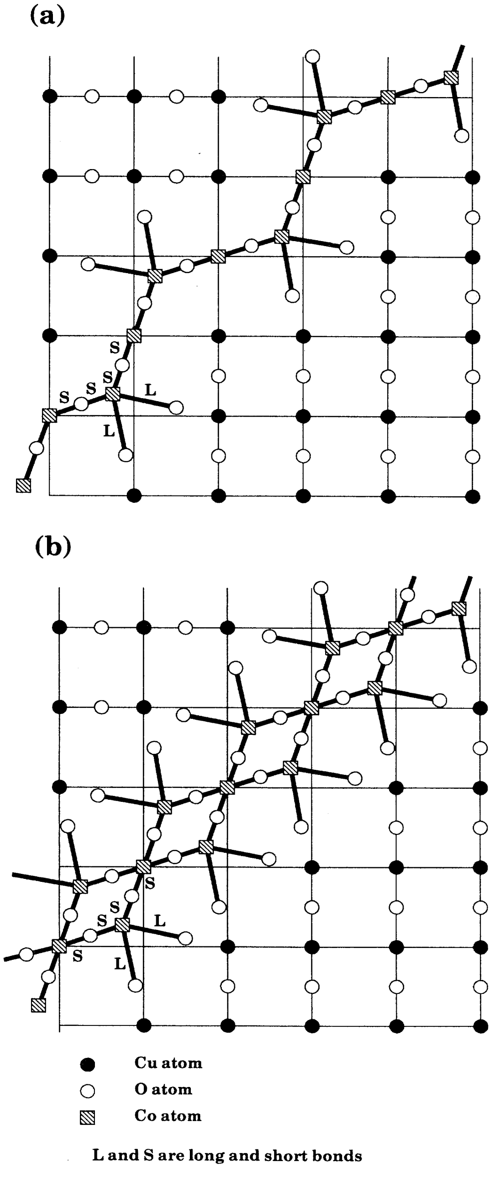

FIG. 11. ⟨110⟩ chainlike clusters propose for Co and Fe in Y-Ba-Cu-O in the Cu chain layer. Some of the Co and O atoms are displaced resulting in short (S) and long (L) Cu-O bonds. From Ref. 6, with permission.

TABLE IV. Co local structure, from the XAFS analysis. For the Co-O nearest neighbors, we have only included two peaks; for a three-peak fit, another Co(1)-O peak appears near 2.02 Å with an amplitude of one neighbor. There are three Co-Ba peaks at r and $r \pm \delta r$. The number of Ba neighbors at the three distances is constrained to be in the ratio 1:4:1 (with the component at a distance r being the largest). In the table, the total number of Ba neighbors is given. The estimated errors are the following: number of neighbors ± 0.5 for Co-O and ± 0.8 for Co-Ba; distances, ± 0.02 Å.

		Co-O		Co-O			Co-Ba	
Sample	Treatment	r (Å)	nbrs	r (Å)	nbrs	r (Å)	δr (Å)	nbrs
5 at. % Co	*U*	1.81	4.0	2.31	0.8	3.56	0.25	8.5
5 at. % Co	*R*	1.83	4.8	2.29	0.8	3.57	0.22	8.5
8 at. % Co	*U*	1.82	4.6	2.27	0.9	3.57	0.28	8.9
8 at. % Co	*R*	1.83	4.4	2.28	0.9	3.58	0.24	8.0
10 at. % Co	*U*	1.82	4.4	2.28	0.8	3.57	0.28	8.8
10 at. % Co	*A*	1.84	4.6	2.30	0.7	3.57	0.24	7.4
10 at. % Co	*R*	1.83	4.8	2.28	0.8	3.58	0.28	8.8
11 at. % Co	*U*	1.83	4.6	2.29	1.0	3.57	0.25	8.5
11 at. % Co	*R*	1.83	4.7	2.28	0.7	3.57	0.25	8.2
30 at. % Co	*U*	1.86	4.6	2.31	0.6	3.56	0.18	7.5
30 at. % Co	*A*	1.85	4.0	2.32	0.6	3.57	0.24	8.9
30 at. % Co	*R*	1.87	4.5	2.31	0.7	3.57	0.19	7.8

In these fits we again find that the main Co-O peak is near 1.83 Å, but is not strongly broadened. A small Co-O peak near 2.3 Å is also needed to obtain a good fit in the r-space region from 1.9 to 2.5 Å. There is a consistent trend that the short Co(1)-O peak lengthens slightly with reoxidation (in agreement with Renevier, Hodeau, and Marezio[8]) and with increasing Co concentration.

The value of δr is comparable in all samples, but shows some trends. For the low-concentration samples, δr decreases slightly with the full thermal processing. For the 10, 11, and 30 at. % Co samples, δr does not change with thermal processing and tends to decrease as the Co concentration increases.

The quality of the fit begins to decrease at 20% of the Co on a Cu(2) site, and at 30 % Co(2), the quality of the fit deteriorates by a factor that ranges from 1.3 to 2.0. In addition, if the fit is started assuming 20% of the Co is on the Cu(2) site and the amplitude for the Co(2)-Y peak is left as a free parameter, the Co(2)-Y amplitude is reduced below the value for 20% Cu(2), for every one of the treated samples. These fits indicate that less than 20% of the Co is on the Cu(2) site, and that the thermal processing does not increase this fraction significantly. The results for the Co-O and Co-Ba bonds are given in Table IV, and the quality of the fit is illustrated in Fig. 12 for the 10 at. % Co sample.

In addition, we also carried out fits with three Co-O peaks below 2.5 Å. The quality of these fits is comparable to the fits with two Co-O peaks, and result in another small peak (corresponding to one O neighbor) near 2.0–2.05 Å, and a drop in amplitude of the 1.83 Å peak, consistent with the results of Renevier, Hodeau, and Marezio.[8] We note that another recent XAFS study[22] finds two Cu(1)-O peaks near 1.75 and 1.88 Å. The short distance agrees with the short Co-O distance we found earlier in a low-Co-concentration (1.7 at. % Co) sample.[6] We discuss these differences later.

Finally we note that the results for the Fe K-edge data (Y-Ba-Cu-O with 7.5 at. % Fe) are similar to the above results for Co substitution. The main Fe-O distance is not as short (1.87–1.9 Å) as for Co-O and the main Fe-Ba peak is at 3.6 Å, with a δr between 0.2 and 0.29 Å for the two samples. Again, there is no evidence for a movement of Fe from a Cu(1) to a Cu(2) site in the reoxidized samples.

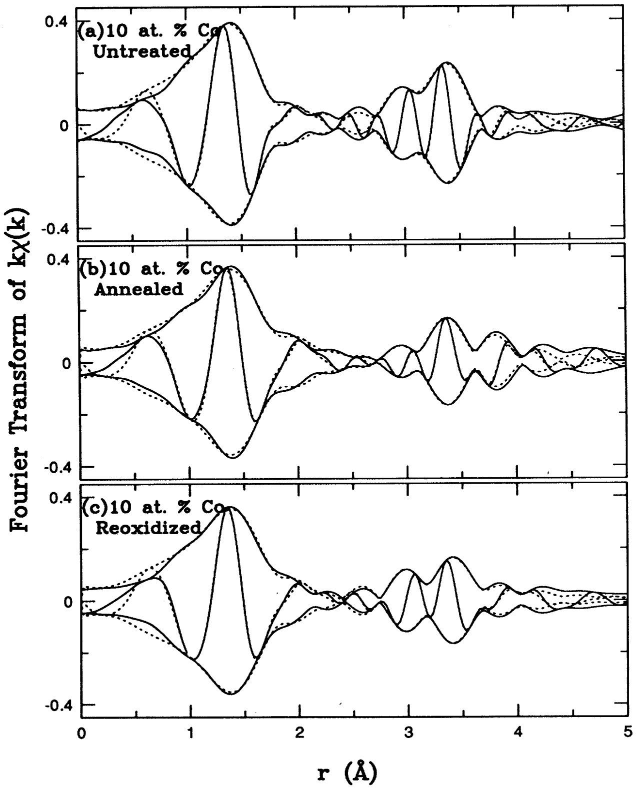

FIG. 12. Fits of the data (Figs. 9 and 10) for the 10 at. % Co samples. Solid line, data; dotted line, fit over range 1–4 Å.

VI. NEAR-EDGE STRUCTURE

In Fig. 13 we show the near-edge structure at the Cu K edge for the untreated, vacuum-annealed, and the reoxidized 10 and 30 at. % Co samples. For both Co concentrations, the data for the untreated and reoxidized samples are identical; i.e., they overlap completely. The main change occurs for the vacuum-annealed sample; when O is removed from the chains, a feature characteristic of a linear twofold-coordinated O-Cu-O configuration is present near 8980 eV, and the average edge moves slightly to lower energy. We use this change in the Cu near-edge structure for the vacuum-annealed samples, relative to the untreated sample, as a measure of the number of twofold-coordinated Cu(1) atoms present. If a large fraction of the Cu(2) and Co(1) atoms were exchanged during the vacuum anneal, then this feature should be large in the 30 at. % Co annealed sample. Using the edge height at 8980 eV as a first measure of the amount of Cu on the Cu(1) sites, plus the assumption that the Co distribution function is similar for the 10 and 30 at. % Co samples, we find that ~10% of the Co is on a Cu(2) site in the high-Co-concentration sample. Since there is also a change in shape, we use the area between the dotted line (vacuum annealed) and the solid line (untreated) as a measure of the maximum amount of twofold-coordinated Cu. Then the amount of Co on a Cu(2) site in the 30 at. % Co sample is $\leq$ 30%. These results are consistent with our XAFS results.

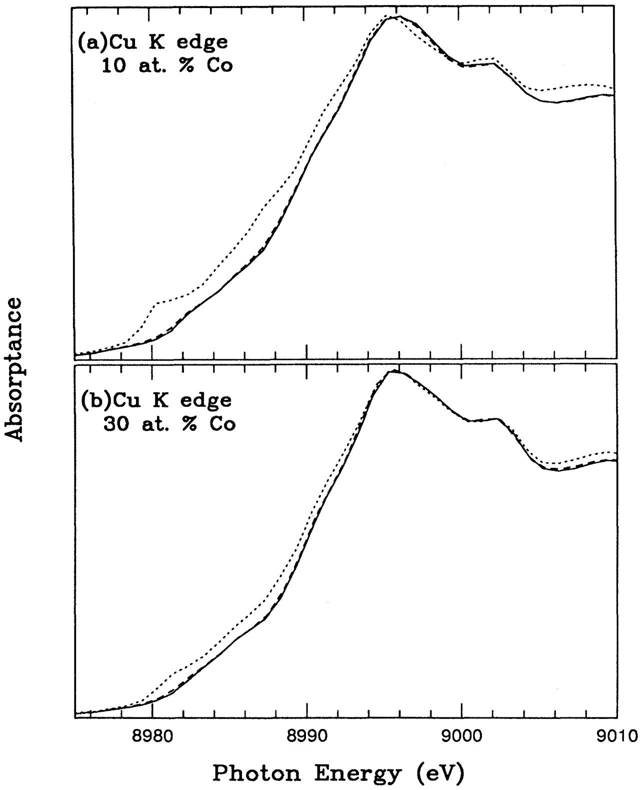

FIG. 13. Near-edge structure at the Cu K edge for the 10 and 30 at. % Co samples. Solid line, untreated; dashed line, reoxidized; dotted line, vacuum annealed. Note the untreated and reoxidized samples are identical.

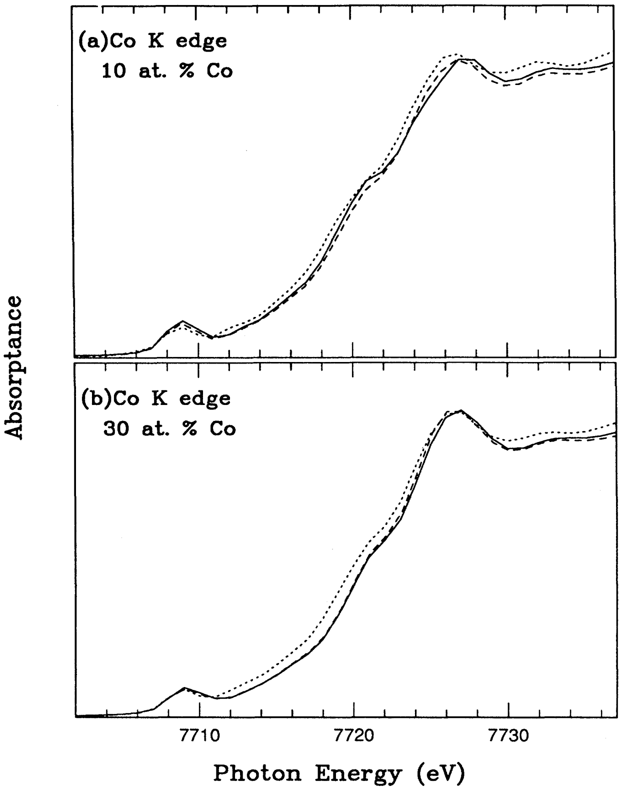

FIG. 14. Near-edge structure at the Co K edge for the 10 and 30 at. % Co samples. Solid line, untreated; dashed line, reoxidized; dotted line, vacuum annealed.

In Fig. 14 the corresponding Co K-edge data shows that there are only small changes in the Co edge between the untreated and reoxidized samples for 10 at.% Co, and essentially no differences for the 30 at. % Co samples. Also there is very little change in the pre-edge peak near 7709 eV, indicating no change in Co valence.[8] These results indicate that the local environment of the Co (i.e., the number of nearest O neighbors) changes very little in the thermal processing, consistent with the small changes in the first O shell of the XAFS data in r space as shown in Fig. 9.

VII. DISCUSSION

Our extensive XAFS investigation of Co-substituted Y-Ba-Cu-O is in general agreement with our earlier results[6] which indicated that Co primarily occupies a strongly distorted Cu(1) site in Y-Ba-Cu-O. The general features of our local structural results are also consistent with the detailed investigation of (untreated) Co-substituted Y-Ba-Cu-O by neutron diffraction[1] [i.e., Co is on the Cu(1) site, there is a contraction of the Cu(2)-Cu(2), a slight expansion of the Cu(1)/Co(1)-Cu(2) distances with Co substitution, etc.] and with anomalous x-ray scattering.[9] Our results are also in substantial agreement with another recent XAFS experiment on Co-substituted Y-Ba-Cu-O by Renevier, Hodeau, and Marezio,[8] but in disagreement with the earlier work of Yang *et al.*[7] and with Padalia *et al.*[22]

We first compare the results of various XAFS studies before considering other experiments. Yang *et al.*[7] found no evidence for a distorted Cu(1) site, but did not carry out a detailed analysis of the further neighbors, which requires doing constrained fits. Since it is the second neighbor shell that shows the main effect of the distortion of the Co(1) site, a fit of only the first neighbor O peak does not provide much information about the local distortions.

Renenier, Hodeau, and Marezio[8] made a more detailed XAFS analysis and also used other techniques. In their XAFS analysis they fit the O shell and the second neighbor shell separately. Our amplitudes and Co-O bond distances agree well with their results when we include three Co-O distances; one of our Co-O peaks (about one neighbor) has a Co-O bond length near 2.3 Å and is important in the region between the oxygen peak and the further neighbor peaks—the region not included in their[8] fits. Thus the differences in the analysis for the O peak are small. For the Co-Ba peaks in the second neighbor shell our main Ba peak is near 3.57 Å, in agreement with our earlier work[6] and the other detailed XAFS study.[8] A short Cu(1)-Cu(1)/Co(1) peak is also observed, in agreement with our earlier work.[6] Further detailed comparisons with Renevier, Hodeau, and Marezio[8] are not possible because they used only a three-peak fit of the second neighbor shell, while we used a constrained, three Ba plus two Cu/Co peak fit. (The imposed constraint is consistent with a ⟨110⟩ Co displacement which results in three Ba peaks.) However, their general results agree very well with ours.

Padalia *et al.*[22] report two different distances for the first O-shell neighbors and use only a single broadened peak for Co-Ba. They argue that because their Co-O peaks are not strongly broadened, they find no evidence for a distorted Co(1) site. We point out that in our analysis, we also find that the Co-O peaks are not broadened very much. It is the *reduced amplitude and change in the structure of the further neighbor multipeak* that indicates the distortion. We find that the structure, consistently observed in the further neighbor multipeak, is not very well described by a single broadened Co-Ba peak. Padalia *et al.*[22] used such a model for their analysis, but do not comment on the very large width ($\sigma \approx 0.14$ Å for the 8 at. % Co sample) required to fit their data. This large width again points to disorder (distortions) in the Co-Ba distances.

For the Fe-substituted sample, our limited results again suggest a distorted Cu(1) site in agreement with recent ion channeling results[33] and theoretical calculations,[34] and we find no evidence for a change of site with thermal processing. The Cu(1) site occupancy for the thermally processed samples agrees with a recent XAFS experiment,[19] but the ⟨110⟩ distorted Fe(1) site, with three Fe(1)-Ba peaks, is at variance with their interpretation. Moodenbaugh *et al.*[19] used a three-peak fit of the second neighbor shell [with a single Fe(1)-Ba peak] for data collected at 300 K. Because of the large Debye-Waller-like factor for 300 K, the amplitude of their high-k data is low compared to our data collected at 80 K (on a $k^3\chi$ plot the relative amplitude difference at 12 Å^{-1} is a factor of 7) and other possibilities were not considered. Padalia *et al.*[22] also investigated Fe-substituted Y-Ba-Cu-O but again used only a single Fe(1)-Ba peak with a large width ($\sigma \approx 0.12$ Å for the 2 at. % Fe sample) to model the further neighbors. They argue that the small broadening of the Fe-O nearest-neighbor distances contradicts the idea of distortion, but they ignore the very large broadening of the further neighbor distances.

The distribution of O atoms about the Co(1) site is likely more complicated than the two- or three-peak structures we and others have used. The small differences in the nearest-neighbor O distances found by different XAFS studies may be a real, sample-dependent effect, indicating that changes in preparation can have a strong effect on the local environment about a Co (or Fe) atom. Theoretical models[34] of the distortions about the Fe atoms in a small cluster in Y-Ba-Cu-O:Fe indicate a range of distances which can be grouped into bond lengths of ≈ 1.8, 2.0, and 2.1 Å, in reasonable agreement with our distorted site model. However, the distances change with the size and type of cluster, and the actual number of distances is more than 3.

Our XAFS and near-edge data both show very little change in structure with the complete thermal process that changes the crystal structure from tetragonal to orthorhombic as determined by x-ray diffraction. Most of the Co remains on the Cu(1) site. We cannot rule out a small amount of Co on the Cu(2) site—our fit results indicate possibly 10% Co(2) (consistent with neutron-diffraction results[1]) with an upper limit of 20–30 % for the 30 at. % Co sample. However, the lack of *change* in the data for the 30 at. % Co sample with thermal processing indicates that *very little additional* Co moves to the Cu(2) site. This is in disagreement with the proposed change of site via annealing in the interpretation of Mössbauer data,[14,17] but in agreement with the interpretation of other experiments.[19,35] Other possibilities have also been considered that ignore a movement from the Cu(1)O chains to the Cu(2)O_2 planes,[36] including clustering[16] or movement into interstitial positions.[20] We also find no evidence for precipitation of Co or Fe oxides—Moodenbaugh *et al.*[19] arrived at the same conclusion for their Fe-substituted samples.

Mössbauer experiments[14,17,18] clearly show a change in the spectra, as a result of the vacuum annealing and reoxidation process, which have been interpreted as a change in substitution site. We propose that there are many distinct Co (and Fe) configurations within the Cu(1) chain sites when the Co(1) site is strongly distorted and clusters have formed. Under the thermal treatment the distribution between different Co configurations (distorted or not distorted, clustered or not clustered, four, five, or sixfold coordinated) must change. The size of any clusters that form will likely vary in size. These changes mostly take place during the vacuum anneal at high temperature (≈ 700 °C); at high temperatures, Co diffuses easily in the *ab* plane but not along the *c* axis.[37]

Our thin-film studies with Fe-substituted Y-Ba-Cu-O show that thermal processing can change T_c substantially and that there are two or more distinct Fe(1) configurations (defects or clusters).[38] Some lead to a higher T_c and an orthorhombic structure as determined by x-ray diffraction while others result in a low T_c and a tetragonal crystal structure. The detailed nature of the Co and Fe defects in Y-Ba-Cu-O are not yet known. However, there is considerable evidence[6,8,33,34] for large distortions of the local environment which may signify a preference for twin or possibly grain boundaries. The reoxidized bulk material discussed here (see Table I) and the thin films deposited at a high substrate temperature both have increased values of T_c, and we think that the local environment may be quite similar.

X-ray-diffraction measurements show that the thermal processing discussed above changes the average crystal structure from tetragonal to orthorhombic for Co (Fe) concentrations below 10–15 at. %. On a local scale, our XAFS results show that this thermal processing results in less disorder about the Cu atoms, and increased disorder of the further neighbors about the Co or Fe atoms. Clearly, in the processed material, the Co (or Fe) atoms have less influence on the Cu local structure, which may explain the higher T_c in most processed material. It is not clear whether this is the result of larger Co (or Fe) clusters or the formation of different sizes or types of clusters. Either might be consistent with the changes observed in Mössbauer spectroscopy.

What are the implications for superconductivity? Changing the thermal processing of Co- and Fe-substituted Y-Ba-Cu-O has a significant effect on T_c of both bulk and thin-film materials. Our results indicate that the processing results primarily in a redistribution of the Co (and Fe) on distorted Cu(1) sites, with the formation of clusters or chains of defect atoms. We think that the strain introduced by clusters is responsible for the suppression of T_c, both through partial charge localization in the Cu(2)O$_2$ planes and changes in the charge transfer between planes and chains. The strain for a large cluster in the chain sites should have a large effect on the Cu(2) sites, whereas the strain introduced by an isolated Cu(1) site may have little effect on the planes. However, a microscopic determination of the defect structure is needed before such conjectures can be tested. The ability to obtain relatively high values of T_c at high concentrations of Co (or Fe) may also be of practical importance if these defects are effective pinning centers.

VIII. CONCLUSION

Our Cu *K*-edge XAFS data show that the Cu local environment is not strongly disordered when Co is partially substituted for Cu in Y-Ba-Cu-O. In particular, the Cu-Ba further neighbor distances (and thus the Ba atom positions in the Y-Ba-Cu-O crystal) are not disordered. In contrast, for the Co *K*-edge data, the further neighbor XAFS peak is significantly reduced, indicating that the further neighbor environment about the Co atoms is strongly distorted or disordered. Our analysis indicates that Co substitutes on the chain [Cu(1)] site and that a large fraction of the Co are displaced relative to the Ba atoms. The main Co(1)-O(1) bond is shortened by roughly 0.1 Å compared to the corresponding Cu(1)-O(1) bond in pure Y-Ba-Cu-O, but it is not strongly broadened. Thus we conclude that CoO$_z$ clusters are displaced relative to the Ba atoms. This distortion is comparable to the distortion we suggested earlier and similar to the results of Renevier, Hodeau, and Marezio.[8]

For each Co concentration (5, 8, 10, 11, and 30 at. %) we investigated the change in local structure after the samples were thermally processed using a high-temperature vacuum anneal (750 °C) followed by a low-temperature (400 °C) anneal in oxygen gas. Some investigators have suggested that this thermal processing moves Co from the chain [Cu(1)] to the plane [Cu(2)] site.

For the Cu *K*-edge data, there is no change in the spectra with this thermal processing for the 30 at. % Co sample. If a significant fraction of the Co had moved to the Cu(2) plane site [and therefore Cu(2) atoms moved to the Cu(1) chain sites] a change in the spectra should have occurred, since the number of oxygen neighbors about the two Cu sites is different, and Cu on the Cu(1) site has no Y neighbors. For the lower Co concentrations, the Cu *K*-edge data is not very sensitive to a possible movement of Co from one site to another. We note that the Cu-Ba peaks are slightly narrower in the thermally processed samples, indicating that the disorder about the Cu atoms has been reduced.

For the Co *K*-edge data, the further neighbors are mainly Ba and Cu/Co, but several Ba peaks are needed, consistent with a ⟨110⟩ displacement of the Co(1) atoms, to fit the data. After thermal processing there is no evidence for the presence of a large Co-Y peak that would indicate that Co has moved to the Cu(2) site. Our low-Co-concentration data are consistent with all the Co on the Cu(1) site; however, we cannot exclude the possibility that a small amount of Co (< 20%) is on the Cu(2) site. The analysis of the data for the 30 at. % Co samples suggests that 10% of the Co may be on the Cu(2) sites.

After the thermal processing, our data show that the Co further neighbors distances become more disordered, in contrast to a more ordered further neighbor environment about the Cu atoms observed in the Cu *K*-edge data. We suggest that this is a result of changes in the size and shape of Co clusters on the Cu(1) sites. This redistribution of Co on the Cu(1) sites leads to a change in crystal structure from tetragonal to orthorhombic, as determined by x-ray diffraction, and usually results in an increase of T_c. The decrease in the disorder of the further neighbors about the Cu atoms after processing indicates that the Co atoms have become less effective in distorting the Cu local environment. We think that the change in T_c is closely linked to this reduction in disorder about the remaining Cu atoms. Similar results were also obtained for one Fe-substituted Y-Ba-Cu-O sample.

ACKNOWLEDGMENTS

We thank Xun Wang for help in data collection. The experiments were performed at the Stanford Synchrotron Radiation Laboratory, which is operated by the U.S. Department of Energy, Division of Chemical Sciences, and by the NIH, Biomedical Resource Technology Program, Division of Research Resources. The work is supported in part by NSF Grant Nos. DMR-90-04325 and DMR-92-05204.

---

[1] R. Sonntag, D. Hohlwein, A. Hoser, W. Prandl, W. Schäfer, R. Kiemel, S. Kemmler-Sack, S. Lösch, M. Schlichenmaier, and A. Hewat, Physica C **159**, 141 (1989).

[2] P. Zolliker, D. E. Cox, J. M. Tranquada, and G. Shirane, Phys. Rev. B **38**, 6575 (1988).

[3] P. F. Miceli, J. M. Tarascon, L. H. Greene, P. Barboux, F. J. Rotella, and J. D. Jorgensen, Phys. Rev. B **37**, 5932 (1988).

[4] Y. Xu, M. Suenaga, J. Tafto, R. L. Sabatini, A. R. Moodenbaugh, and P. Zolliker, Phys. Rev. B **39**, 6667 (1989).

[5] Q. Lin, P. L. Zhang, Z. G. Shen, D. S. Tang, Q. W. Yan *et al.*, Solid State Commun. **82**, 389 (1992).

[6] F. Bridges, J. B. Boyce, T. Claeson, T. H. Geballe, and J. M. Tarascon, Phys. Rev. B **39**, 11603 (1989).

[7] C. Y. Yang, A. R. Moodenbaugh, Y. L. Wang, Y. Xu, S. M. Heald, D. O. Welch, M. Suenaga, D. A. Fischer, and J. E. Penner-Hahn, Phys. Rev. B **42**, 2231 (1990).

[8] H. Renevier, J. L. Hodeau, and M. Marezio, in *Lattice Effects in High-T_c Superconductors*, edited by Y. Bar-Yam, T. Egami, J. Mustre de Leon, and A. R. Bishop (World Scientific, New Jersey, 1992), p. 118.

[9] R. S. Howland, T. H. Geballe, S. S. Laderman, A. Fischer-Colbrie, M. Scott, J. M. Tarascon, and P Barboux, Phys. Rev. B **39**, 9017 (1989).

[10] M. Kakihana, L. Börjesson, S. Eriksson, P. Svedlindh, and P. Norling, Phys. Rev. B **40**, 6787 (1989).

[11] L. C. Sengupta, B. Roughani, J. Aubel, S. Sundaram, and W. C. H. Joiner, Physica C **165**, 125 (1990).

[12] B. Roughani, L. C. Sengupta, J. Aubel, S. Sundaram, and W. C. H. Joiner, Physica C **171**, 77 (1990).

[13] C. Blue, K. Elgaid, I. Zitkovsky, P. Boolshand, D. McDaniel, W. C. Joiner, J. Oostens, and W. Huff, Phys. Rev. B **37**, 5905 (1988).

[14] S. Nasu, M. Yoshida, Y. Oda, K. Asayama, F. E. Fujita, T. Kohara, S. Katsuyama, Y. Ueda, K. Kosuge, T. Shinjo, and I. S. Lyubutin, Physica C **185-189**, 865 (1991).

[15] E. Takayama-Muromachi, Y. Uchida, and K. Kato, Jpn. J. Appl. Phys., **26**, L2087 (1987).

[16] S. Katsumyama, Y. Ueda, and K. Kosage, Physica C **165**, 404 (1990); H. Mazaki, S. Katsuyama, H. Yasuoka, Y. Ueda, and K. Kosage, Jpn. J. Appl. Phys. **28**, L1909 (1989).

[17] M. G. Smith, R. D. Tayor, and H. Oesterreicher, Phys. Rev. B **42**, 4202 (1990).

[18] Z. Q. Qui, Y. W. Du, H. Tang, and J. C. Walker, J. Appl. Phys. **67**, 5458 (1990).

[19] A. R. Moodenbaugh, C. Y. Yang, Y. Zhu, R. Sabatini, D. A. Fischer, Y. Xu, and M. Suenaga, Phys. Rev. B **44**, 6991 (1991).

[20] A. Nath, Z. Homonnay, S. Tyagi, Y. Wei, G.-W. Jang, and C. Chan, Physica C **171**, 406 (1990).

[21] M. G. Smith, J. B. Goodenough, A. Manthiram, R. D. Tayor, and H. Oesterreicher, Phys. Rev. B **46**, 3041 (1992).

[22] B. D. Padalia, S. J. Gurman, P. K. Mehta, and O. Prakash, J. Phys. Condens. Matter. **4**, 6865 (1992).

[23] T. M. Hayes and J. B. Boyce, in *Solid State Physics*, edited by H. Ehrenreich, F. Seitz, and D. Turnbull (Academic, New York, 1982), Vol. 37, p. 173.

[24] E. A. Stern and S. M. Heald, in *Handbook on Synchrotron Radiation*, edited by E. E. Koch (North-Holland, New York, 1983), Vol. 1, p. 955.

[25] F. Bridges, Nucl. Instrum. Methods A **257**, 447 (1987).

[26] J. B. Boyce, F. Bridges, T. Claeson, and M. Nygren, Phys. Rev. B **39**, 6555 (1989).

[27] J. B. Boyce, F. G. Bridges, T. Claeson, T. H. Geballe, G. G. Li, and A. W. Sleight, Phys. Rev. B **44**, 6961 (1991).

[28] J. Mustre de Leon, J. J. Rehr, S. I. Zabinsky, and R. C. Albers, Phys. Rev. B **44**, 4146 (1991).

[29] G. G. Li, F. Bridges, and G. Brown, Phys. Rev. Lett. **68**, 1609 (1992).

[30] M. A. Beno, L. Soderholm, D. W. Capone II, D. G. Hinks, J. D. Jorgensen *et al.*, Appl. Phys. Lett. **51**, 57 (1987).

[31] C. C. Torardi, E. M. McCarron, P. E. Bierstedt, A. W. Sleight, and D. E. Cox, Solid State Commun. **64**, 497 (1987).

[32] J. D. Jorgensen, B. W. Veal, A. P. Paulikas, L. J. Nowicki, G. W. Crabtree, H. Claus, and W. K. Kwok, Phys Rev. B **41**, 1863 (1990).

[33] L. Romano, M. Brees, D. Jamieson, C. Chen, G. Grime, and F. Watt, Phys. Rev. B **44**, 6927 (1991).

[34] M. S. Islam and C. Ananthamohan, Phys. Rev. B **44**, 9492 (1991).

[35] M. Matsumura, H. Yamagata, and Y. Oda, Physica C **185-189**, 1135 (1991).

[36] D. Hechel, I. Nowik, E. Bauminger, and I. Felner, Phys. Rev. B **42**, 2166 (1990).

[37] J. L. Routbort, S. J. Rothman, N. Chen, J. N. Mundy, and J. E. Baker, Phys. Rev B **43**, 5489 (1991).

[38] F. Bridges, J. B. Boyce and R. Johnson, Appl. Phys. Lett. **60**, 3042 (1992).